Journal of Applied Polymer Science

# Morphology, Mechanical, and Rheological Properties of Poly(lactic acid)/Ethylene Acrylic Acid Copolymer Blends Processing via Vane Extruder

**Yong-Qing Zhao,[1,2] Fu-Quan Chen,[1,2] Zheng-Huan Wu,[1,2] Yan-Hong Feng,[1,2] Jin-Ping Qu[1,2]**

[1]National Engineering Research Center of Novel Equipment for Polymer Processing, South China University of Technology, Guangzhou 510640, Guangdong, People's Republic of China

[2]The Key Laboratory of Polymer Processing Engineering of Ministry of Education, South China University of Technology, Guangzhou 510640, Guangdong, People's Republic of China

Correspondence to: J.-P. Qu (E-mail: jpqu@scut.edu.cn)

**ABSTRACT:** This work aimed to study, for the first time, the melt blending of poly(lactic acid) (PLA) and ethylene acrylic acid (EAA) copolymer by a novel vane extruder to toughen PLA. The phase morphologies, mechanical, and rheological properties of the PLA/EAA blends of three weight ratios (90/10, 80/20, and 70/30) were investigated. The results showed that the addition of EAA improves the toughness of PLA at the expense of the tensile strength to a certain degree and leads the transition from brittle fracture of PLA into ductile fracture. The 80/20 (w/w) PLA/EAA blend presents the maximum elongation at break (13.93%) and impact strength (3.18 kJ/m$^2$), which is 2.2 and 1.2 times as large as those of PLA, respectively. The 90/10 and 80/20 PLA/EAA blends exhibit droplet-matrix morphologies with number average radii of 0.30–0.73 $\mu$m, whereas the 70/30 PLA/EAA blend presents an elongated co-continuous structure with large radius (2.61 $\mu$m) of EAA phase and there exists PLA droplets in EAA phase. These three blends with different phase morphologies display different characteristic linear viscoelastic properties in the low frequency region, which were investigated in terms of their complex viscosity, storage modulus, loss tangent, and Cole-Cole plots. Specially, the 80/20 PLA/EAA blend presents two circular arcs on its Cole-Cole plot. So, the longest relaxation time of the 80/20 blend was obtained from its complex viscosity imaginary part plot, and the interfacial tension between PLA and EAA, which is 4.4 mN/m, was calculated using the Palierne model. © 2013 Wiley Periodicals, Inc. J. Appl. Polym. Sci. **2014**, *131*, 40146.

**KEYWORDS:** biodegradable; blends; morphology; rheology; mechanical properties

Received 16 June 2013; accepted 30 October 2013

**DOI: 10.1002/app.40146**

## INTRODUCTION

Increasing concerns over the environmental influence and sustainability of conventional polymer materials have motivated academia and industry to devote considerable efforts to the development of biodegradable polymers from renewable resources.[1,2] One of the most promising biobased and biodegradable polymers considered for commodity applications is poly(lactic acid) (PLA), which is an aliphatic polyester derived from renewable resources such as corn starch and sugar cane through fermentation and ring-opening polymerization, and will hydrolyze to harmless natural products when disposed of properly.[3] Despite its numerous advantages such as high strength and stiffness, the inherent brittleness significantly impedes its wide applications in many fields, such as packaging, textile, and automotive industries. To improve its toughness, the blends of the PLA with other flexible polymers or rubbers, such as poly(butylene succinate) (PBS),[4,5] poly($\varepsilon$-caprolactone),[6] linear low-density polyethylene,[7] and thermoplastic polyurethane (TPU),[8] have been investigated. For example, Han and Huang[8] reported that the 70/30 (w/w) PLA/TPU blend exhibits a much higher value of elongation at break than pure PLA. However, among these polymers, many had high price, reduced biodegradability, or caused poor compatibility; these disadvantages limit the applications of these blends in certain areas.[4–8]

Ethylene acrylic acid copolymer (EAA) is commonly used as packing material, powder coat, adhesive, hot melt glue.[9,10] In addition, EAA was proposed as compatibilizer for some binary immiscible blends, such as, polypropylene (PP)/thermotropic liquid crystalline polymer,[11–13] low density polyethylene/polyamide 6,[14,15] and poly(butylene terephthalate)/ethylene vinyl acetate copolymer blends.[16] EAA was also blended with other polymers and fillers.[17–19] For example, the addition of EAA into PP/carbon black (CB) composites can improve the electrical conductivity of PP/CB composites significantly, and the

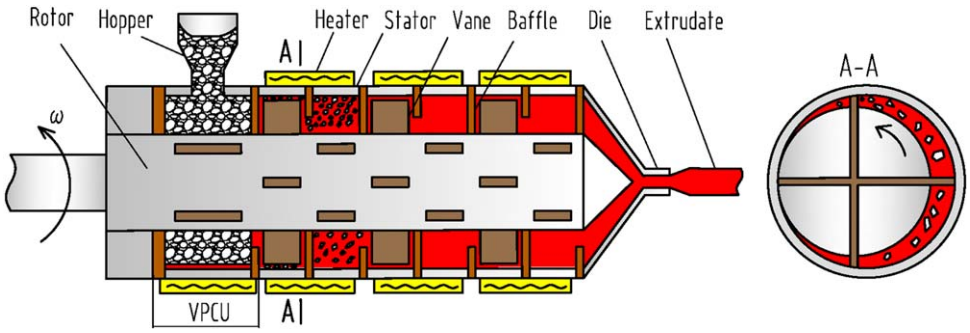


**Figure 1.** Structure schematic diagram of vane extruder. [Color figure can be viewed in the online issue, which is available at wileyonlinelibrary.com.]

dynamic rheological properties of PP/EAA/CB blends were also studied.[18]

However, from a thorough literature survey, it was noticed that there was no report on EAA toughening other brittle polymers, although it presents high toughness and flexibility. For a given binary polymer blend, the interfacial properties between the two components play an important role in their phase morphology and mechanical properties. So, this work aimed to, for the first time, toughen PLA by melt blending with EAA. The morphologies, mechanical and dynamic rheological properties of the PLA/EAA blends were also investigated. Moreover, the interfacial tension between PLA and EAA in the blends was estimated from the morphology and dynamic rheological properties of the PLA/EAA blends.

## EXPERIMENTAL

### Materials and Equipment

As the matrix phase, PLA (grade 2003D, NatureWorks LLC) with a melt temperature of 157°C, a melt flow index of 8.8 g/10 min (210°C, 2.16 kg), and a density of 1.24 g/cm$^3$ was used. EAA (grade 2014, DuPont company) with a melt temperature of 86°C, a melt flow index of 7.9 g/10 min (190°C, 2.16 kg), and a density of 0.94 g/cm$^3$ was used as the dispersed phase.

The vane extruder invented by Qu,[20,21] is a non-screw processing equipment dominated by elongational deformation. Its structure schematic diagram is presented in Figure 1. The vane extruder is mainly constituted by seven vane plasticizing and conveying units (VPCU) as shown in Figure 1. Each group of VPCU is composed of a stator, a rotor, four vanes, and two baffles, which is used for feeding, processing, and discharging materials. The rotor is eccentrically installed in the intracavity of the stator. The four vanes are installed in pairs in the rectangular through hole of the rotor. When the rotor is rotating, the pair of vanes makes a reciprocating movement through the radial rectangular through hole of the rotor because of the action of the inner surface of the stator. This action leads to the periodic changing of the volume constituted by the stator, rotor, two adjacent vanes, and two baffles. The VPCU feeds materials from the front VPCU through the feed baffle when the volume increases, whereas it discharges materials to the next VPCU through the discharge baffle when the volume decreases. The process involves grinding, compressing, venting, and melting. These operations take place simultaneously rather than sequentially. In the vane extruder, the discharge baffle of the front VPCU is the feed baffle of the next one. In two adjacent VPCUs, the eccentric directions of the rotor are opposite, that is, in the second VPCU, the rotor is eccentric to the left and is eccentric to the right in the third VPCU. In this way, the discharge outlet of the front VPCU connects with the feeding inlet of the next VPCU to complete a continuous dynamic plasticating and conveying process. Moreover, to reduce the discharge fluctuation, the locations of the vanes change to an angle of 45° in two adjacent VPCUs.[20–25] The vane extruder can provide an elongational field to produce a good mixing under lower shear intensity, which is favorable for processing the biodegradable polyesters.

### Sample Preparation

PLA and EAA were dried at (80°C and 50°C) for 8 h in a vacuum oven, respectively. The PLA/EAA blends were mixed and extruded by a vane extruder at a rotating speed of 30 rpm. The profile temperatures were (165°C, 180°C, 180°C, 180°C, and 180°C), respectively. Three PLA/EAA blends with (10, 20, and 30 g)/100 g EAA were prepared. For comparison, the pure PLA and EAA were also processed under the same conditions. The blend strands for scanning electron microscope (SEM) observation were collected from the die exit and quenched in iced water quickly. The disks with a diameter of 25 mm and a thickness of about 2 mm for dynamic rheological measurements of the blends and pure materials were immediately compressed from the melt just out of the die exit and also quenched in iced water quickly. Then, all the prepared samples for SEM observation and dynamic rheological measurement were dried at 50°C for 8 h in a vacuum oven. In addition, the blend and pure PLA strands were cut into granules and then compression molded into the pieces with a thickness of (1 and 4 mm) by using a flat sulfuration machine (model QLB-25D/Q, China) at 10 MPa and 180°C for 6 min, the sheets were cooled to room temperature about 30°C, removed from the mold, and then cut into the test bars. The bars were conditioned at 50% relative humidity and 25°C for at least 48 h before testing.

### Characterization

Tensile tests were carried out on the prepared blend and pure PLA samples using an Instron Universal Testing Machine (model 5566). Crosshead speed and gauge length were 10 mm/

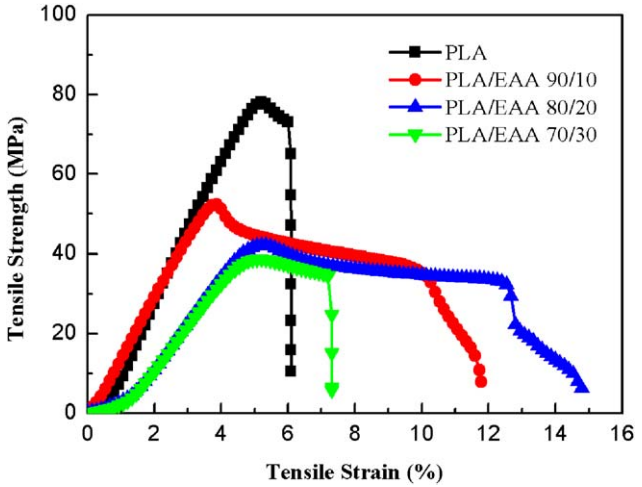


**Figure 2.** Tensile stress–strain curves for PLA/EAA blends with various weight ratios and pure PLA. [Color figure can be viewed in the online issue, which is available at wileyonlinelibrary.com.]

min and 70 mm, respectively. Notched Izod impact tests for the prepared blend and pure PLA samples were conducted using a Zwick Impact Tester (model 5117, Germany) with a pendulum hammer of 5.4 J. The tensile strength, tensile modulus, elongation at break, and impact strength were determined as an average of at least five repeats.

Dynamic rheological properties of the blends and pure materials were measured using a Bohlin Rheometer (model Gemini 200, UK) equipped with a parallel-plate fixture (25 mm diameter) in an oscillatory mode. The complex viscosity ($\eta^*$), storage modulus ($G'$), and loss modulus ($G''$) as a function of angular frequency ($\omega$) ranging from 0.0628 to 628 rad/s were measured by frequency sweep at 180°C. Before conducting the frequency sweep, amplitude sweep was performed at a controlled strain mode from 0.01% to 100% at a frequency of 6.28 rad/s and a temperature of 180°C to determine a fixed strain of 1%, which was used to ensure that the frequency sweep was carried out within the linear viscoelastic range of the samples investigated.

The previously prepared blend strands were immersed in liquid nitrogen for about 15 min and fractured perpendicular to the flow direction. Then they were gold sputtered and their cryo-fractured surfaces were examined using a FEI SEM (model Quanta 200, Holland) at an accelerating voltage of 20 kV. On analyzing the SEM micrographs of the blend samples, the volume and number average radii ($R_v$, $R_n$) of the droplets were calculated by:

$$R_V = \frac{\sum_i n_i R_i^4}{\sum_i n_i R_i^3} \quad (1)$$

$$R_n = \frac{\sum_i n_i R_i}{\sum_i n_i} \quad (2)$$

where $R_i$ is the radius of each droplet, and $n_i$ is the number of droplets with $R_i$.

### Statistical Analysis

The means and standard deviations of the data were calculated for each treatment. ANOVA was carried out to determine any significant difference ($P < 0.05$) among the applied treatments using SPSS software (SPSS 10.0 for windows).

## RESULTS AND DISCUSSION

### Mechanical Properties

The stress–strain curves for the PLA/EAA blends with various weight ratios and pure PLA are displayed in Figure 2. As can be seen, pure PLA has a high stiffness and a poor toughness. Moreover, pure PLA exhibits a distinct yield point, beyond which failure occurs immediately with the tensile load, whereas all of the blends appear as a continuous development of deformation after yield, and their stress–strain curves present a stress platform of elastic deformation. In addition, the phenomena of stress-whiting were observed for all blends during their tensile tests. These results indicate that facture behavior changes from brittle fracture of PLA to ductile fracture of the blends.

Table I displays the tensile strength, tensile modulus, elongation at break, and impact strength for the PLA/EAA blends with various weight ratios and pure PLA. As can be seen, the pure PLA displays a high tensile strength (75.66 MPa) and a low elongation at break (6.45%). With increasing of EAA content from 10 to 30 wt %, the tensile strength for the blends decreases gradually from 52.92 to 39.49 MPa. However, the elongation at break for the blend increases rapidly with the addition of 10 wt % EEA, reaches a maximum value of 13.93% with 20 wt % EEA, and exhibits a little decrease with further increase in the EAA content. The impact strength for pure PLA is 2.56 kJ/m$^2$. The impact strength for the blends increases with the increase of the EAA content from 10 to 20 wt % and exhibits a little decrease with further increase in the EAA content. When the EAA loading is 20 wt %, it attains a maximum of 3.18 kJ/m$^2$.

The tensile and impact testing results indicate that the addition of EAA improves the toughness of PLA at the expense of the tensile strength to a certain degree, and the 80/20 PLA/EAA blend presents preferable mechanical properties compared with other two blends. The decrease in the tensile strength of blends, on the one hand, is due to the lower tensile strength of EAA; on the other hand, it may be because of the weak interactions between the PLA and EAA phases. In addition, the mechanical properties of blends are strongly related to the phase morphology and interfacial tension. The phase morphologies and dynamic rheological properties of these three blends were also

**Table I.** Mechanical Properties for PLA/EAA Blends with Various Weight Ratios and Pure PLA

| PLA/EAA blend (w/w) | Tensile strength (MPa) | Tensile modulus (MPa) | Elongation at break (%) | Impact strength (kJ/m$^2$) |
|---|---|---|---|---|
| 0/100 | 75.55$^a$ | 1953.75$^a$ | 6.45$^a$ | 2.566$^a$ |
| 90/10 | 52.92$^b$ | 1695.76$^b$ | 12.91$^c$ | 2.702$^a$ |
| 80/20 | 41.06$^c$ | 1205.39$^c$ | 13.93$^d$ | 3.178$^b$ |
| 70/30 | 39.49$^d$ | 1150.46$^d$ | 7.99$^b$ | 2.471$^a$ |

Means in the same column with the same letter are not significantly different ($P < 0.05$).

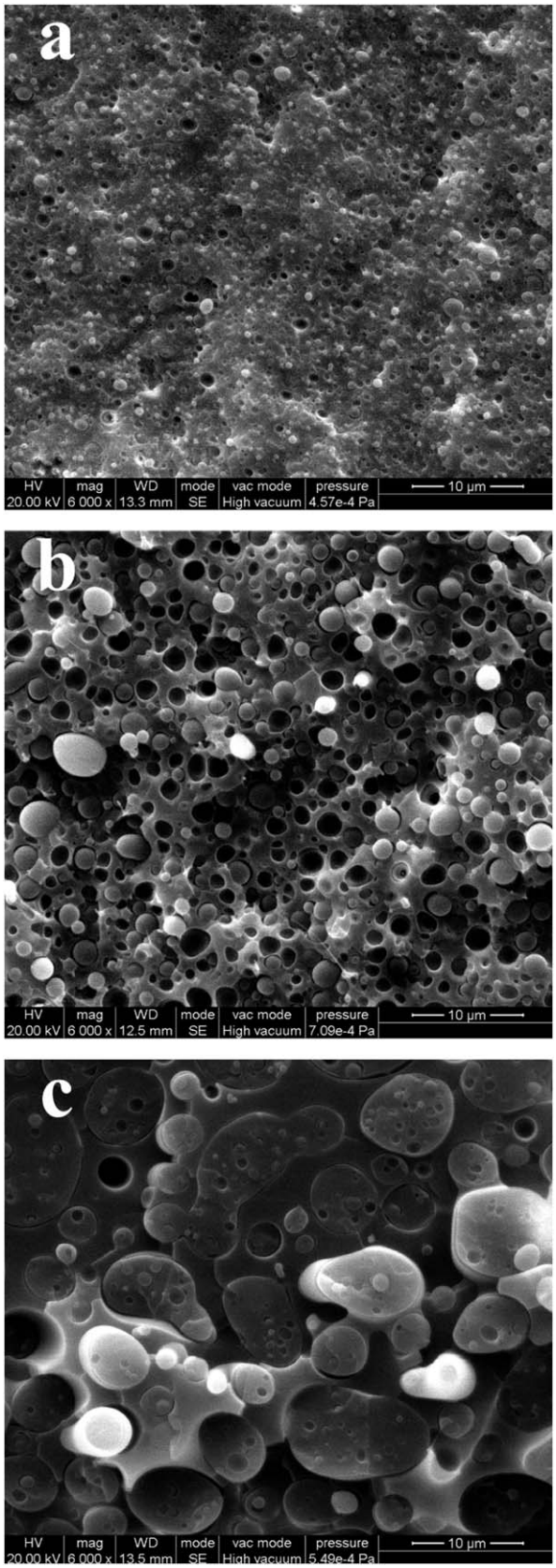


**Figure 3.** SEM micrographs of PLA/EAA blends with various weight ratios (w/w), (×6000): (a) 90/10, (b) 80/20, and (c) 70/30.

**Table II.** $R_n$ and $R_V$ of EAA Droplets for 90/10 and 80/20 Blends and EAA Phase and PLA Droplets for 70/30 Blend

| PLA/EAA blend (w/w) | 90/10 | 80/20 | 70/30 | |
|---|---|---|---|---|
| | | | EAA phase | PLA droplets |
| $R_n$ ($\mu$m) | 0.53 | 0.73 | 2.61 | 0.31 |
| $R_V$ ($\mu$m) | 0.67 | 0.93 | 3.59 | 0.44 |

investigated. Based on these results, the interfacial tension between the PLA and EAA phases was calculated.

### Phase Morphology

Figure 3 illustrates the SEM micrographs on the fractured surfaces for the prepared PLA/EAA blends with various weight ratios. As can be directly observed, the 90/10 and 80/20 (w/w) PLA/EAA blends exhibit droplet-matrix morphologies, whereas the 70/30 PLA/EAA blend presents an elongated co-continuous structure[26] and there exists PLA droplets in EAA phase. This may be attributed to the fact that the vane extruder provides an elongational flow,[20–25] which can produce an elongated co-continuous structure. In addition, the EAA melts prior to the PLA, and small PLA droplets may be trapped inside the EAA phase during the inversion process.[27] Figure 3 also shows that the 90/10 blend shows an ambiguous interface, whereas the 80/20 blend presents a clear interface of the EAA and PLA phases, which indicates that the former blend has a certain degree of miscibility, whereas the latter blend is immiscible.

The $R_V$ and $R_n$ of the EAA droplets in PLA phase for the 90/10 and 80/20 blends, EAA phase and PLA droplets for the 70/30 blend calculated by eqs. (1) and (2) are listed in Table II. As can be seen, the $R_n$ of the EAA droplets in the 90/10 and 80/20 PLA/EAA blends are 0.30 and 0.73 $\mu$m, respectively. The $R_n$ of the PLA droplets in the 70/30 PLA/EAA blend is only 0.31 $\mu$m, whereas the $R_n$ of the EAA phase in the PLA matrix is 2.61 $\mu$m, which maybe the reason for the poor mechanical properties of

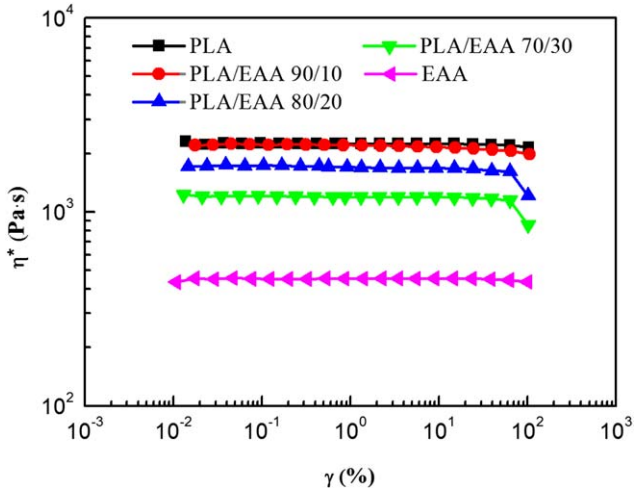


**Figure 4.** Complex viscosity versus strain for PLA/EAA blends with various weight ratios and pure PLA and EAA at 180°C. [Color figure can be viewed in the online issue, which is available at wileyonlinelibrary.com.]

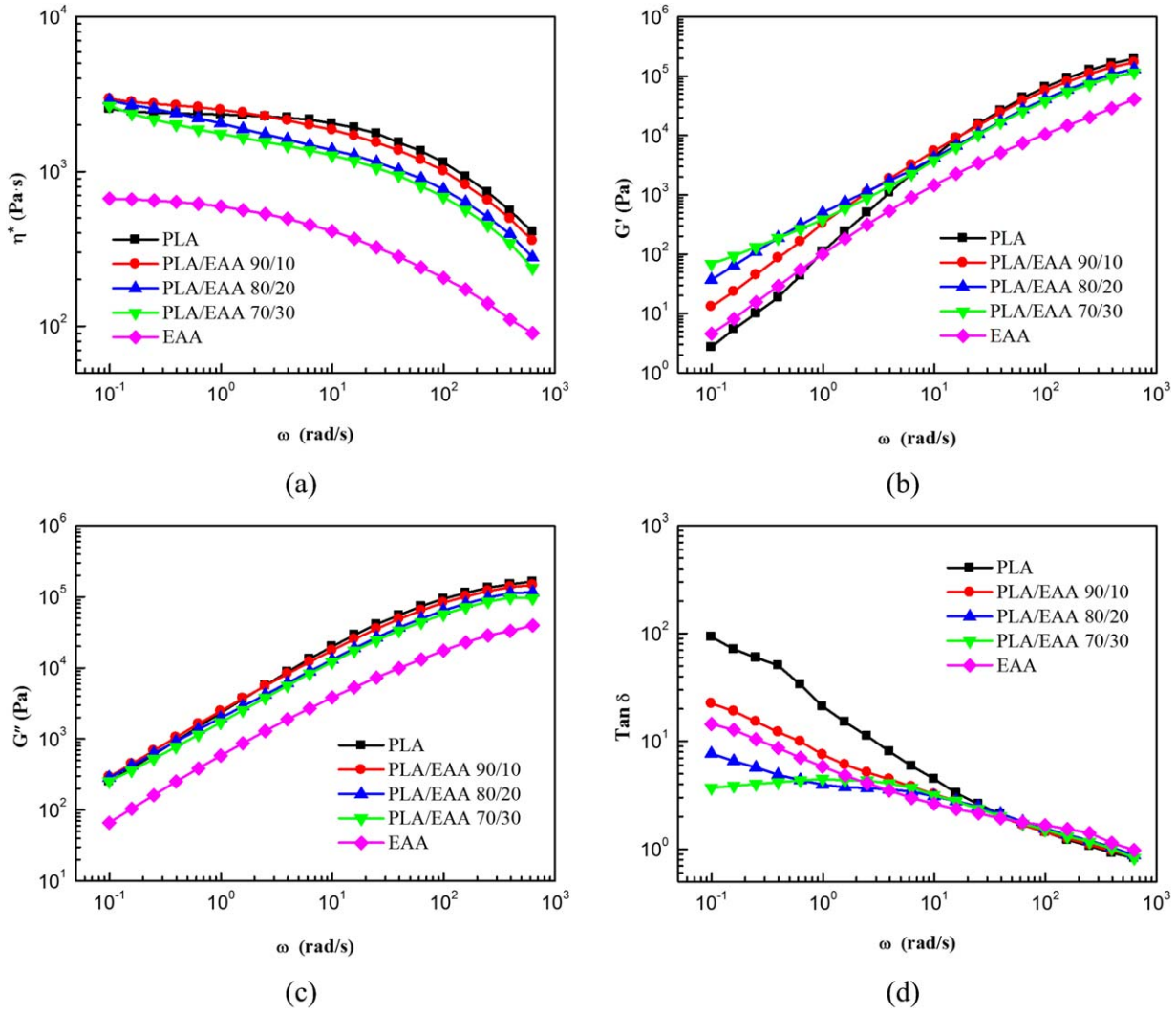


**Figure 5.** (a) Complex viscosity, (b) storage modulus, (c) loss modulus, and (d) loss tangent versus angle frequency for PLA/EAA blends with various weight ratios and pure PLA and EAA at 180°C. [Color figure can be viewed in the online issue, which is available at wileyonlinelibrary.com.]

the 70/30 PLA/EAA blend compared with the 80/20 PLA/EAA blend.

### Dynamic Rheological Properties

To ensure that the frequency sweep was carried out within the linear viscoelastic range of the samples investigated, the amplitude sweep was performed on the PLA/EAA blends with various weight ratios and pure PLA and EAA at 180°C, and the $\eta^*$ versus strain ($\gamma$) plots of these samples are shown in Figure 4. It can be clearly seen that the $\eta^*$ values of these samples keep constant in the strain range of 0.01% to 14.9%. In this work, the strain of amplitude sweep was fixed at 1%. Further observing Figure 4, it is clearly visible that the values of $\eta^*$ for pure PLA are higher than that for pure EAA, and the values of the $\eta^*$ for the blends decrease gradually with the increase of the EAA loading.

Figure 5 shows the $\eta^*(\omega)$, $G'(\omega)$, $G''(\omega)$, and loss tangent ($\tan\delta = G'/G''$) plots for the PLA/EAA blends with various weight ratios and pure PLA and EAA at 180°C. It can be clearly seen from Figure 5(a) that the values of $\eta^*$ for pure PLA are higher than that for pure EAA, and so the values of the $\eta^*$ for the blends decrease gradually with the increase of the EAA loading. It is interesting to note that the values of the $\eta^*$ for all the blends are higher than those of the pure PLA and EAA in the low frequency region. Moreover, compared with the pure PLA and EAA, the blends begin to exhibit the shear thinning behavior at lower frequencies, and the frequency decreases with increasing the EAA loading. These phenomena may be attributed to the relaxation of the deformed droplets, and were also observed for other blends, such as PLA/PBS,[5] and PLA/poly(butylenes adipate-*co*-terephthalate) blends.[28]

As shown in Figure 5(b), the $G'(\omega)$ plots of the blends are located between those of the pure PLA and EAA in the high frequency region, whereas the values of $G'(\omega)$ of the blends are larger than those of both pure components in the low frequency region. Moreover, with increased EAA loading, the values of the $G'$ of the blends in the high- and low-frequency regions decrease and increase, respectively. These can be explained briefly as follows. There exist two relaxation processes reflected on the $G'(\omega)$

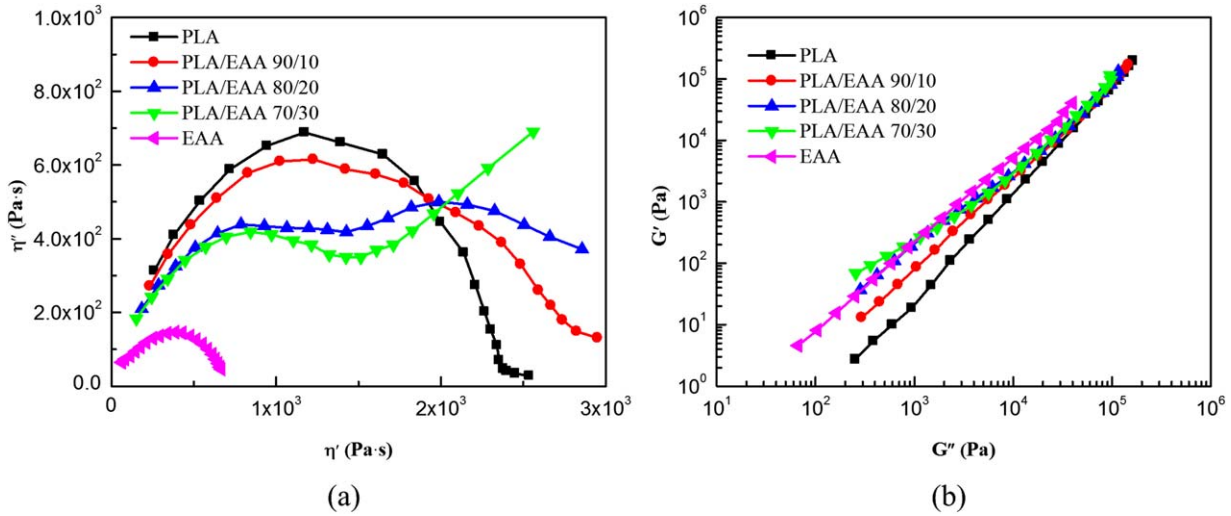


**Figure 6.** (a) Cole-Cole and (b) modified Cole-Cole plots of PLA/EAA blends with various weight ratios and pure PLA and EAA at 180°C. [Color figure can be viewed in the online issue, which is available at wileyonlinelibrary.com.]

plots in the whole tested frequency range: one is for the relaxation of the blend in the high frequency region and the other for the relaxation of the deformed dispersed droplets for the blend with droplet-matrix morphology and for the network relaxation of interpenetrating phases for the blend with co-continuous structure in the low frequency region.[26] Higher EAA loading leads to lower blend viscosity and generates less elastic energy,[29] resulting in a lower $G'$ value in the high frequency region. Increasing EAA loading increases the deformation degree of the dispersed droplets,[29,30] which increases the elastic energy generated by their deformation and thus the value of the $G'$ in the low frequency region. The power law behavior of the $G'(\omega)$ plot in the low frequency region for the blend with co-continuous structure leads to higher value of the $G'$ when compared to the blend with droplet-matrix morphology.[26] The $G''(\omega)$ plots of the blends are located between those of the pure PLA and EAA in the high frequency region and close to the $G''(\omega)$ plot of PLA in the low frequency region, as shown in Figure 5(c).

It can be seen from Figure 5(d) that the values of the tan$\delta$ for all the blends and pure components are close to each other in the high frequency region, whereas in the low frequency, the tan$\delta(\omega)$ plot of the 90/10 (w/w) PLA/EAA blend is located between those of the pure components, and the values of the tan$\delta$ for the 80/20 and 70/30 PLA/EAA blends are lower than those for the pure components. Moreover, there exist a plateau and a peak on the tan$\delta(\omega)$ plots of the 80/20 and 70/30 PLA/EAA blends, respectively. The plateau on the tan$\delta(\omega)$ plots for the 80/20 blend is a typical result of the relaxation for the deformed dispersed droplets.[31] The appearance of the peak may be attributed to the network relaxation of interpenetrating phases for the 70/30 blend with co-continuous structure.

Since the immiscible blends with different phase morphologies exhibit different relaxation mechanisms, their Cole-Cole plots that describe the relationship between the imaginary part $\eta''$ ($=G'/\omega$) and real part $\eta'$ ($=G''/\omega$) of the $\eta^*$ should display different shapes. Figure 6 displays the Cole-Cole plots of the prepared PLA/EAA blends and pure components, in which the modified Cole-Cole plots[32] of the prepared PLA/EAA blends and pure components are also given. It can be seen from Figure 6(a) that the 90/10 PLA/EAA blend as well as pure PLA and EAA only presents one circular arc on their Cole-Cole plots, indicating that the blend is partially miscible and consistent with the result of the morphology observation. Figure 6(a) also shows that there exists a circular arc and a tail in the low-frequency region on the Cole-Cole plots for 80/20 and 70/30 PLA/EAA blends, respectively, which should be the characteristic reflections of the different morphologies; that is, the droplet-matrix and co-continuous morphologies should be responsible for such features.[33] Figure 6(a) also shows that the circular arcs in the high frequency region of the Cole-Cole plots of the blends are located between those of the pure components, and their radii decrease with the increase of the EAA loading. Since the blend viscosity decreases with increasing EAA loading, there is less elastic energy and therefore smaller radii of the circular arcs in the high frequency region of the Cole-Cole plots.

The modified Cole-Cole plot of the PLA/EAA blends displays a composition-dependent correction, as shown in Figure 6(b), indicating that the PLA/EAA blends are immiscible.[34] The slope of the modified Cole-Cole plot in the low-frequency range for the PLA/EAA blend decreases with increasing EAA loading. It is understandable due to the aforementioned relaxation of the dispersed EAA.

### Interfacial Tension of PLA and EAA

Palierne[35] proposed a linear viscosity constitutive equation for the binary immiscible blend with droplet-matrix morphology as a function of the linear viscosity of the two components, the size distribution of the dispersed droplets and the interfacial tension. Assuming that the droplet size distribution is narrow ($R_V/R_n < 2.3$) and the interfacial tension between the components is independent of the local deformation of the interface, Graebling et al.[36] simplified the Palierne model. Moreover, for a binary immiscible blend, Graebling et al.[36] defined the longest relaxation time of the blend ($\lambda_D$) and corresponds to the total shape relaxation of the droplets, which can be calculated using the following equations:

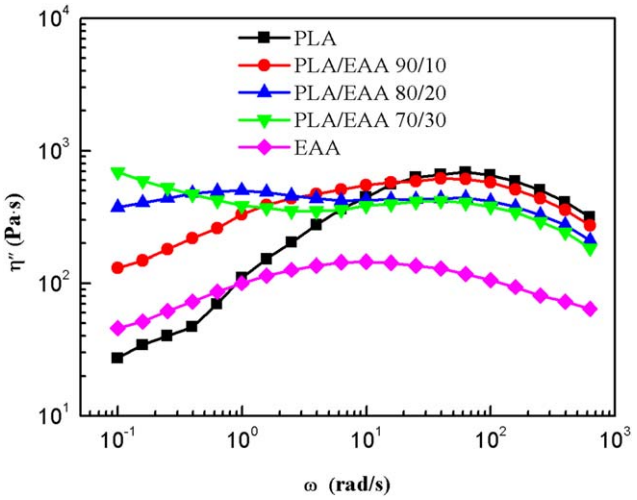


**Figure 7.** Imaginary part of complex viscosity versus angle frequency of PLA/EAA blends with various weight ratios and pure PLA and EAA at 180°C. [Color figure can be viewed in the online issue, which is available at wileyonlinelibrary.com.]

$$\lambda_D = \frac{R_V \eta_{0,m}}{4\alpha} \frac{(19K+16)[2K+3-2\varphi(K-1)]}{10(K+1)-2\varphi(5K+2)} \quad (3)$$

where $K = \eta_{0,i}/\eta_{0,m}$ is the zero-shear viscosity ratio of the dispersed phase and matrix; $\varphi$ is the volume fraction of the dispersed phase; $\alpha$ is the interfacial tension between the components of the blend.

Based on the results of the PLA/PBS blend, Xu and Huang[5] suggested that the reciprocal of the frequency corresponding to the peak in the low-frequency region on the $\eta''(\omega)$ plot for the binary immiscible blend was defined as its longest relaxation time, and the interfacial tension between the two phases of the PLA/PBS blend is calculated using eq. (3).

Figure 7 shows the $\eta''(\omega)$ plots of the PLA/EAA blends with various weight ratios and pure PLA and EAA at 180°C. As can be seen, only the 80/20 PLA/EAA blend displays two peaks on its $\eta''(\omega)$ plot, while the 90/10 PLA/EAA blend as well as pure PLA and EAA only present one circular arc, and 70/30 PLA/EAA blend shows a tail and a circular arc in the low- and high-frequency regions on their $\eta''(\omega)$ plots, respectively. So in this work, the calculation of the interfacial tension between PLA and EAA was conducted only for the 80/20 PLA/EAA blend. The longest relaxation time of the 80/20 PLA/EAA blend is obtained from its $\eta''(\omega)$ plot, which is 1.0 s.

In the calculation of the interfacial tension, $R_V$, $\eta_{0,i}$, and $\eta_{0,m}$ should be used. Using the values of the $R_V$ and $R_n$ of the dispersed EAA droplets for the 80/20 PLA/EAA blend given in Table I, the $R_V/R_n$ is calculated, which is equal to 1.28 and does not exceed a value of about 2.3 as mentioned above. The $\eta_{0,i}$ and $\eta_{0,m}$ are calculated by[37]:

$$\eta_0 = \lim_{\omega \to 0} \frac{G''}{\omega} \quad (4)$$

The calculated value of the interfacial tension between the PLA and EAA is 4.4 mN/m. The calculated value of the interfacial tension between the PLA and EAA is consistent with the SEM micrographs, and the medium value results in the 80/20 blend with a clear interface of the EAA and PLA phases.

## CONCLUSIONS

To improve the toughness of PLA, the PLA/EAA blends with three different weight ratios were prepared by a vane extruder, and their morphology, mechanical, and dynamic rheological properties were investigated. The results showed that the elongation at break and impact strength of the blends increase with the addition of EAA, and then decrease slightly with further increase in the EAA content. The 80/20 PLA/EAA blend presents preferable mechanical properties compared with 70/30 PLA/EAA blend, which maybe because the former blend displays droplet-matrix morphology with small radius (0.73 $\mu$m) of EAA droplets, while the latter one presents an elongated co-continuous structure with large radius (2.61 $\mu$m) of EAA phase.

The complex viscosity for pure PLA is higher than that for pure EAA, and so the complex viscosities of the blends decrease gradually with the increase of the EAA loading. Interestingly, the blends with three types of phase morphologies show different characteristic linear viscoelastic behaviors in the low frequency region. The 90/10 blend presents droplet-matrix morphology with ambiguous interface of the two components and one circular arc on its Cole-Cole plot. The 80/20 blend shows droplet-matrix morphology with clear interface, and the relaxations of the deformed dispersed droplets leads to a shoulder on its storage modulus and loss tangent plots, and two circular arcs on its Cole-Cole plot. In addition, the network relaxation of interpenetrating phases for the 70/30 PLA/EAA blend induces the appearance of a power law behavior on the storage modulus plot, a peak on the loss tangent plot, and a large tail on its Cole-Cole plot in the low frequency region.

The calculation of the interfacial tension between the PLA and EAA was conducted on the 80/20 PLA/EAA blend, and the calculated result is 4.4 mN/m. This is consistent with the SEM micrographs, and the medium value of the interfacial tension between the PLA and EAA results in the 80/20 blend with a clear interface of the EAA and PLA phases.

## ACKNOWLEDGMENTS

This research was supported by grants from National Nature Science Foundation of China-Guangdong Joint Foundation Project (U1201242); National Nature Science Foundation of China (51373058); Program for New Century Excellent Talents in University (NCET-11–0152); Pearl River Talent Fund for Young Sci-Tech Researchers of Guangzhou City (2011J2200058).

## REFERENCES

1. Demirbas, A. *Energy Sources Part A* **2007**, *29*, 419.
2. Zhang, J. W.; Liu, H. Z. *J. Polym. Sci. Polym. Phys.* **2011**, *49*, 1051.
3. Garlotta, D. *J. Polym. Environ.* **2001**, *9*, 63.
4. Shibata, M.; Inoue, Y.; Miyoshi, M. *Polymer* **2006**, *47*, 3557.
5. Xu, L. Q.; Huang, H. X. *J. Appl. Polym. Sci.* **2012**, *125*, E272.

6. Simoes, C. L.; Viana, J. C.; Cunha, A. M. *J. Appl. Polym. Sci.* **2009**, *112*, 345.
7. Anderson, K. S.; Lim, S. H.; Hillmyer, M. A. *J. Appl. Polym. Sci.* **2003**, *89*, 3757.
8. Han, J. J.; Huang, H. X. *J. Appl. Polym. Sci.* **2011**, *120*, 3217.
9. Luo, N.; Michael, J. S.; Douglas, E. H. *J. Appl. Polym. Sci.* **2004**, *92*, 1688.
10. Su, J.; Chen, S.; Zhang, J.; Xu. Z. Z. *J. Reinf. Plast. Comp.* **2010**, *29*, 2946.
11. Mandal, P. K.; Chakraborty, D. *J. Appl. Polym. Sci.* **2009**, *111*, 2345.
12. Mandal, P. K.; Siddhanta, S. K.; Chakraborty, D. *J. Appl. Polym. Sci.* **2011**, *119*, 1034.
13. Mandal, P. K.; Siddhanta, S. K.; Chakraborty, D. *J. Appl. Polym. Sci.* **2012**,*124*, 5279.
14. Canfora, L.; Filippiand, S.; La Mantia, F. P. *Polym. Eng. Sci.* **2004**, *44*, 1732.
15. La Mantia, F. P.; Canfora, L.; Dintcheva, N. T. *Polym. Eng. Sci.* **2005**, *45*, 1297.
16. Scaffaro, R.; La Mantia, F. P.; Castronovo, C. *Macromol. Chem. Phys.* **2004**, *205*, 1402.
17. Pethe, V. V.; Wang, H. P.; Hiltner, A.; Baerand, E.; Freeman, B. D. *J. Appl. Polym. Sci.* **2008**, *110*, 1411.
18. Chen, G. S.; Yang, B.; Guo, S. Y.; *J. Polym. Sci. Polym. Phys.* **2009**, *47*, 1762.
19. Chen, S. J.; Zhang, J.; Su, J. *J. Appl. Polym. Sci.* **2009**, *112*, 1166.
20. Qu, J. P. *Can. Pat. CN200810026054*, **2009**.
21. Qu, J. P. *Eur. Pat. EP2113355*, **2013**.
22. Qu, J. P.; Zhang, G. Z.; Chen, H. Z.; Yin, X. C.; He, H. Z. *Polym. Eng. Sci.* **2012**, *52*, 2147.
23. Qu, J. P.; Zhao, X. Q.; Li, J. B.; Cai, S. Q. *J. Appl. Polym. Sci.* **2013**, *127*, 3923.
24. Qu, J. P.; Liu, L. M.; Tan, B.; Liu, S. R.; Chen, H. X.; Feng, Y. H. *Polym. Compos.* **2012**, *33*, 185.
25. Qu, J. P.; Yang, Z. T.; Yin, X. C.; He, H. Z.; Feng. Y. H. *Polym. Plast. Technol. Eng.* **2009**, *48*, 1270.
26. Potschke, P.; Paul, D. R. *J. Macromol. Sci. Polym. R* **2003**, *C43*, 87.
27. Sundararaj, U.; Macosko, C. W. *Polym. Eng. Sci.* **1996**, *36*, 1769.
28. Li, K.; Peng, J.; Turng, L. S.; Huang, H. X. *Adv. Polym. Technol.* **2011**, *30*, 150.
29. Bousmina, M. *Rheol. Acta* **1999**, *38*, 251.
30. Omonov, T. S.; Harrats, C.; Moldenaers, P.; Groeninckx, G. *Polymer* **2007**, *48*, 5917.
31. Peón, J.; Vega, J. F.; Del Amo, B.; Martínez-Salazar, J. *Polymer* **2003**, *44*, 2911.
32. Ahmad, Z.; Rasekh, M.; Edirisinghe, M. *Macromol. Mater. Eng.* **2010**, *295*, 320.
33. Li, R.; Yu, W.; Zhou, C. X. *J. Macromol. Sci. Phys.* **2006**, *45*, 889.
34. Kim, J.; Kim, J. H.; Shin, T. K.; Choi, H. J.; Jhon, M. S. *Eur. Polym. J.* **2001**, *37*, 2131.
35. Palierne, J. F. *Rheol. Acta* **1990**, *29*, 204.
36. Graebling, D.; Muller, R.; Palierne, J. F. *Macromolecules* **1993**, *26*, 320.
37. Ferry, J. D. Viscoelastic Properties of Polymers, 3rd ed.; Wiley: New York, **1980**.